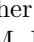


Masked Image Modeling as a Framework for Self-Supervised Learning across Eye Movements

Robin Weiler^{1,*}, Matthias Brucklacher ^{1,*}, Cyriel M. A. Pennartz¹, and Sander M. Bohte^{1,2}

¹ Cognitive and Systems Neuroscience Group, University of Amsterdam, Science Park 904, 1098XH Amsterdam, Netherlands

² Machine Learning Group, CWI Amsterdam, Science Park 123, 1098 XG Amsterdam, Netherlands
matthias.brucklacher@gmail.com

Abstract. To make sense of their surroundings, intelligent systems must transform complex sensory inputs to structured codes that are reduced to task-relevant information such as object category. Biological agents achieve this in a largely autonomous manner, presumably via self-supervised learning. Whereas previous attempts to model the underlying mechanisms were largely discriminative in nature, there is ample evidence that the brain employs a generative model of the world. Here, we propose that eye movements, in combination with the focused nature of primate vision, constitute a generative, self-supervised task of predicting and revealing visual information. We construct a proof-of-principle model starting from the framework of masked image modeling (MIM), a common approach in deep representation learning. To do so, we analyze how core components of MIM such as masking technique and data augmentation influence the formation of category-specific representations. This allows us not only to better understand the principles behind MIM, but to then reassemble a MIM more in line with the focused nature of biological perception. From a theoretical angle, we find that MIM disentangles neurons in latent space, a property that has been suggested to structure visual representations in primates, without explicit regulation. Together with previous findings of invariance learning, this highlights an interesting connection of MIM to latent regularization approaches for self-supervised learning. The source code is available under <https://github.com/RobinWeiler/FocusMIM>

Keywords: Self-supervised learning · Representation learning · Generative model

* Equal contribution

1 Introduction

Both biological and artificial intelligent systems must construct useful object representations (in the general case equivalent to classifiable) from large amounts of unlabeled data [1]. In self-supervised learning (SSL), two main approaches have crystalized over the last years: multi-view based learning (via contrasting [2], latent regularization [3] or distillation [4]), and masked image-modeling (MIM) [5, 6] which predicts occluded image content usually at the pixel-level, but to which also the more recently developed latent predictions [7] can be counted. While constrastive methods have been suggested as a model of SSL in the brain, structuring representational geometry via temporal [8] and spatial cues [9], we postulate that the brain may be engaged in MIM via eye movements and attention shifts (Fig. 1): Perception, at a singular point in time, is selective, both through foveal vision and selective attention [10]. But perception is also dynamic: saccadic eye movements and attention shifts flood the sensory stream with new information - in a manner that is to some degree predictable from knowledge about the direction and magnitude of the gaze shift (via a corollary discharge [11, 12]) and image structure.

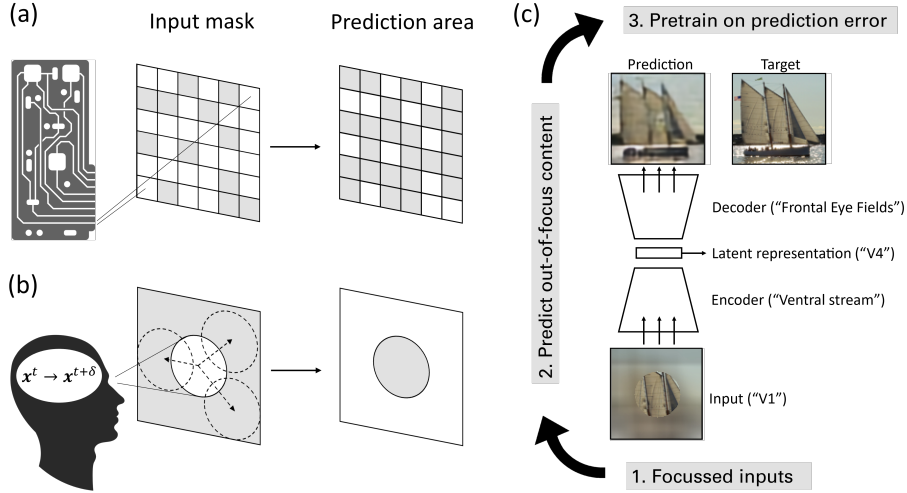


Fig. 1. Representation learning through eye-movements. (a) Random patch masks used in artificial MIM approaches, gray patches are hidden from the network. (b) In our approach, selective masking is achieved through the inhomogeneous nature of foveal vision. Eye movements depicted as vectors reveal previously inaccessible or distorted information that is compared to the prediction $x^t \rightarrow x^{t+\delta}$. (c) After pretraining on the prediction task, the quality of latent representations in the latent representation is assessed through classification accuracy in linear probing.

Studying the principles behind MIM is attractive as it requires less assumptions about temporal sequences and data augmentations than the mentioned multi-view approaches to biological SSL. Furthermore, such an approach fits well with predictive theories of cortical processing [13–15]: both predictive processing [16] and MIM [17] conceptualize perception as the process of identifying a hierarchical latent variable model that could have caused the sensory inputs (this generative aspect is lacking in discriminative SSL models) and are predictive of future inputs. Experimentally, the frontal eye fields have been proposed to stabilize perception through predictions across eye movements [11]. We postulate a larger role of this mechanism: the learning of visual features useful for downstream tasks such as classification.

Here, we investigate the influence of multiple variations to MIM in convolutional neural networks (CNNs) that align well with biological constraints. First, the influence of different masking strategies is tested, resulting in a peripheral masking strategy that learns strong representations and is more in line with the focused nature of biological perception. In doing so, we discover that representations are markedly improved, and that neurons become more decorrelated, when peripheral information is completely suppressed during learning. Second, the influence of data augmentation is tested, showing that these are especially relevant for the peripheral masking strategy. Third, we show that the relevant loss signal originates from the main object: although networks reconstruct the context too, this is not necessary for representation learning. In fact, we find that under some conditions networks learn faster when being only rewarded for predicting the foreground, which is interesting as segmentation may naturally be available from geometric cues or motion [18, 19]. Indeed, availability of segmentation has been shown to aid contrastive SSL if leveraged during pretraining [20], while its effect on MIM has previously not been studied to our knowledge.

2 Related Work

The breakthrough for MIM in representation learning arguably was achieved using random patch masks (Fig. 1a) in a vision transformer [6], an architecture that differs from information processing in biological networks. Subsequently, Kong et al. [17] and He et al. [6] found that an optimal learning ratio falls roughly between 40% and 80%, being sufficiently large but not overly aggressive.

A more biologically compatible CNN for MIM was developed by [5]. The authors found that a central mask (predicting from peripheral context to a small central region) performed worse than randomly distributed patch or region masks, although quantitative reports were not provided. A more recent CNN-based MIM is ConvNext-V2 [21], which utilizes random patch masks like the transformer-based methods in combination with a shallow decoder. Xie et al. [22] further demonstrated the potential for MIM in CNNs, achieving high accuracy in a ResNet-based model. Neither Woo et al. [21] nor Xie et al. [22]

investigated a classical self-supervised paradigm with limited amounts of labeled data and instead finetuned the pretrained model on the full ImageNet dataset used during pretraining.

Biological approaches to SSL derive mostly from multi-view approaches. They avoid representation collapse, a catastrophic network state in which different inputs are projected onto the same latent activity pattern and thus cannot be distinguished anymore, by introducing an expanding force that pushes representations apart. Illing et al. [9] used a single negative sample at a time, interpreted as being obtained by larger eye movements. Their approach converts contrastive predictive coding [2] into a fully local learning rule. Interestingly, the model also has a generative component (predicting the next representation in a sequence of views) as a means to representation learning that is not investigated further. Local predictive learning (LPL) [8], on the other hand relies on pushing representations apart based on their temporal distance, converting variance regularization [3] into a local learning rule. In contrast, MIM as we employ it, prevents representation collapse in a more minimalist way, i.e., without the necessity of negative examples [9] or accumulative temporal statistics [8], and instead solving a generative problem in which loss minimization is incompatible with a collapsed solution. As the approach presented here is an initial step, we use the spatially non-local backpropagation, however, see [23, 24] and subsequent work for biologically plausible solutions yielding comparable weight updates.

Focused vision has been combined with eye movements for functional benefits in a variety of ways, from information gain in line with active inference [25], to achieving representation invariance and reducing the need for detail when learning a generative model [26]. The model of Thompson et al. [27] combines spatially structured eye-movements with visual information processing in an enactive approach to counting. The abovementioned model of Illing et al. [9] uses on- vs. off-object eye movements as a heuristic to shape representation distances in latent space. In comparison, our approach is more reduced in dynamics and focuses instead on the consequences for neural representation learning when casting eye movements as a self-supervised predictive task.

3 Method

3.1 Model

We reduce the task of predicting across eye-movements to its essence and avoid the burden of learning a spatial transformation, which we argue is orthogonal to the process of information restoration that drives representation learning [17]. As a consequence, inputs and predictions take place in the same reference frame (Fig. 1c), as in other MIM approaches [6, 17, 21]. The network architecture shown in Fig. 1c resembles an autoencoder where an encoder network maps input images to a compressed latent code from which a decoder network reconstructs the image. The encoder reduces the spatial dimension from 96x96 (with three

color channels) to a spatial bottleneck of 12×12 (with 128 channels), forming the so called latent representation. Due to the large receptive fields of the latent space neurons at the output of the encoder, they map roughly onto neurons in visual area V4 or higher in primates [28]. From here, the inversely structured decoder (with deconvolutions instead of convolutions) maps the latent representations back onto a $96 \times 96 \times 3$ output that constitutes the model’s expectation of image content. Both encoder and decoder consist of nine ResNet18-style blocks [29] in three stages without batch normalization layers, as convolutional networks are closer to biological networks than transformers.

3.2 Self-Supervised Pretraining

As other work in MIM, we define pretraining as the self-supervised training phase in which the model is presented with a partial view of an image and attempts to predict the image pixel by pixel in full resolution. The loss function is given as the mean squared reconstruction error in parts of visual space with incomplete inputs (masked or blurred, depending on the paradigm), normalized by the area over which the loss is calculated. This reconstruction loss is reminiscent of generative model learning in predictive coding [14]. Pretraining was conducted on the unlabeled split of the STL-10 dataset [30], which was specifically constructed for SSL. We investigated different masking strategies illustrated in Fig. 2 as inputs during pretraining:

Random patches: The most common masking strategy used, e.g., in [17, 21, 29] (see also Fig. 1a). In our implementation, we split the image into 144 patches of 8×8 pixels and replaced the masked image content with the average color of the image.

Masked periphery: A central circle in full resolution with the periphery filled in the sample’s average color (see also Fig. 1b). Biologically, this strict discarding of out-of-focus information is imaginable through inattentiveness [10].

Blurry periphery and **Blurry random patches:** Variations of the above paradigms with Gaussian-blurred information instead of average colors.

Fovea filter: The circular center (“fovea”) of the image is in full resolution with a very small radius. The further out from the center a pixel is, the higher the level of blur, mimicking the physiological constraints of human foveal vision, i.e., the distribution of cone photoreceptors across the retina [31, p. 244]. We follow the implementation of [32, 33] by means of a resolution map determining the blur filter’s spatial frequency at a given distance from the center.

For both random patches and masked periphery (using a square mask instead of a circle), we experimented with sparse convolutions as in [21] to avoid processing of borders between masks and image content. However, we found no significant difference in linear probing accuracy (as described below), so we continued

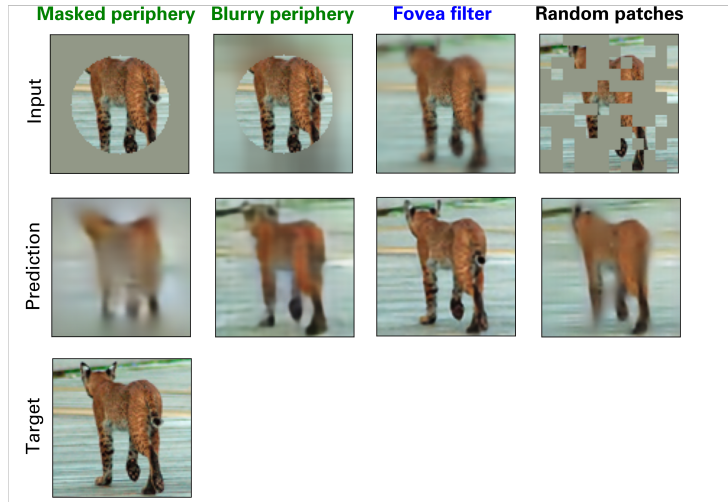


Fig. 2. The masking strategies define the pretraining task. Top row: Exemplary inputs for different pretraining paradigms with masked areas covered in the image’s gray average color. Masked periphery and random patches are shown with 60% masking ratio. Middle row: Predictions from the given inputs after pretraining. Bottom image: Ground truth.

with standard convolutions. During pretraining, we employed random-resized cropping (scale $\in [0.08, 1.0]$, aspect ratio $\in [0.75, 1.33]$). We used the ADAM optimizer [34] (weight decay=1e-8, batch size=512) and selected the learning rate from [5e-5, 1e-4, 5e-4] that led to the best classification performance (described below) for each of the major pretraining tasks (masked periphery, random patches, foveal filter). This value was then kept when blurry information was introduced. After 500 epochs of pretraining, we continued with the model achieving the lowest reconstruction loss for further analysis.

3.3 Linear Probing

To analyze the quality of the learned representations after pretraining, linear probing was conducted. Here, we followed the standard procedure common in SSL of discarding the decoder and appending a linear layer to the frozen encoder. The 128x12x12x10 (latent dimension * classes of the STL-10 labeled splits) parameters of the linear layer were then fit without further augmentations on the training split of the STL-10 dataset (5,000 images), of which we used 1,000 for training validation and early stopping. We used images without mask or blurring, as these consistently led to higher readout accuracy. As in pretraining, we employed the ADAM optimizer [34] (learning rate=1e-4, weight decay=1e-8, batch size=512). Classification accuracy was then evaluated on the 8,000 test images, averaged across five randomly seeded runs. We also experimented with

multilayer perceptron readout and finetuning (retraining the whole network), but neither of these approaches led to large differences in accuracy.

3.4 Correlation of Neurons in Latent Space

In addition to linear discriminability, representations can also be analyzed based on their statistical properties. One desirable property here is decorrelation [3, 35, 36]. To quantify this, the covariance matrix is required [3, 36]:

$$C(R) = \frac{1}{n-1} \sum_{i=1}^n \mathbf{r}_i \mathbf{r}_i^T \quad (1)$$

with R defined as a tensor containing the n latent representation vectors \mathbf{r}_i (that are z-scored across the batch dimension), with n equal to the number of samples, in our case $n = 100,000$. As in [3], the sum of the squared off-diagonal entries in C then quantifies the degree to which neurons are correlated:

$$c(R) = \sum_{i \neq j} [C(R)]_{i,j}^2 \quad (2)$$

3.5 Disentangling Predictions of Object vs. Background

Unlike in the pretraining paradigms outlined so far, eye movements do not reveal all previously unavailable information at once. Instead, they usually fall on salient points, often objects [37, 38]. Objects may also be segmented already before recognition, either from motion signals [19], occlusion geometry, or both [18], making them the prioritized prediction targets. We thus evaluated the influence of reduced learning signal availability from the background. First, we obtained a figure-background segmentation mask using the *rembg*-library (<https://github.com/danielgatis/rembg>). We discarded images in which less than 100 pixels (out of 96x96) received a confidence score of 0.8 (out of 1) or higher. In these $\sim 8,000$ images, no clear segmentation mask was obtained. Otherwise, as shown in Fig. 3, the masks were generally high-quality and only small object parts were missed. During pretraining, the reconstruction loss was then multiplied with the mask value (between 0 and 1) at each point in space and normalized to account for the reduced prediction area.

3.6 Determining the Optimal Masking Ratio

For each of the major masking paradigms, we varied the masking ratio to choose a model with optimal classification accuracy. For the random patches, we found a masking ratio of 60% to lead to the best representations. For the masked periphery, a higher ratio of 80% performed slightly better. We thus continued with this fraction for the remaining results and refer to [17, 29] for more detailed studies on the influence of the masking ratio.

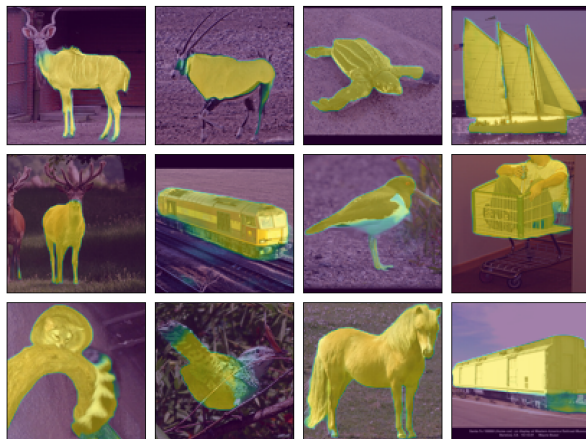


Fig. 3. Representative presegmentation masks used to investigate how discarding loss signals from the background affects network performance, obtained with *rembg*. Displayed are the masks obtained with the *rembg*-library, with brightness indicating confidence, overlayed onto the respective STL-10 images.

4 Results

We applied various combinations of masking strategy and data augmentation, the results of which are shown in Fig. 4.

4.1 Influence of Masking Strategy

Out of the used masking strategies, we identified the masked periphery condition as the most promising candidate for a biological model. This masking technique inspired by foveal visual perception led to the second highest classification accuracy in linear readout (mean value $67.9 \pm 0.4\%$) when crop-and-resize transformations were used during pretraining, outperformed only by the random patch-wise masks ($70.2 \pm 0.4\%$). Strong performance in these settings supports the assumption that solving the pretraining tasks of predicting hidden image areas leads to discovery of object representations [17]. In contrast, deblurring the peripheral region from the foveal filter resulted in comparably poor representations with readout accuracy not much higher than pure autoencoding. Presumably, this condition allows the network to find a local solution that does not require a globally integrated representation. To more closely investigate the effect of input information content on classification accuracy, we introduced Gaussian blurred information in the masked areas (Fig. 2, third column) of the masked periphery and random patch masks. Despite the low information content, the introduced information was sufficient to degrade performance substantially (Fig. 4c).

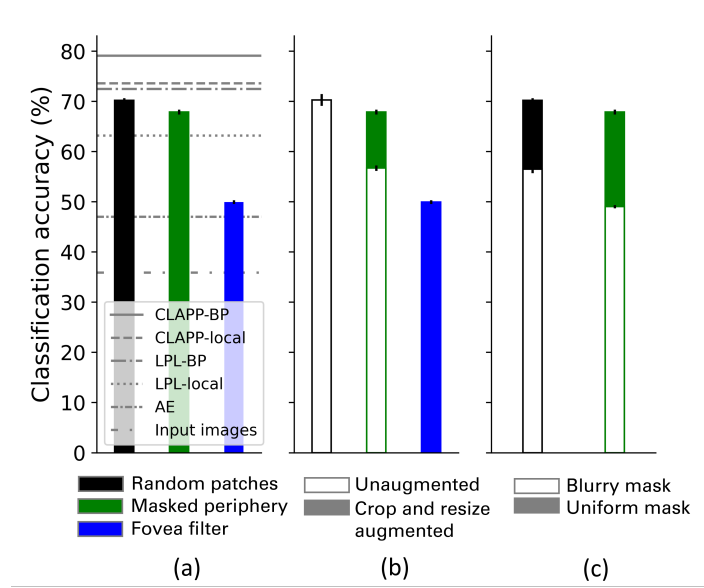


Fig. 4. Linear readout accuracy quantifies representation quality after pretraining. a) Influence of masking strategy in comparison to the multi-view approaches CLAPP [9] and LPL [8], that both come in two variants trained with a local learning rule or backpropagation. The remaining baselines are pure autoencoding (AE) from full image to full image in the same network as the masked methods, and directly conducting linear probing on the input images. b) Influence of data augmentation. In the left- and rightmost bar, the filled and outlined bars overlap, i.e., classification accuracy is unaffected by augmentation. c) Incomplete masking by Gaussian blurring, instead of uniform average coloring, drastically decreases representation quality. Error bars indicate the standard deviation across five randomly seeded runs.

4.2 Decorrelation of Latent Space Neurons

To investigate the degree to which neurons in latent space develop independent tuning properties, we computed the correlation term c using Eq. 2. Interestingly, both masked periphery and random patches decorrelate neural representations (Fig. 5), and more strongly than the foveal filter. This decorrelation, reminiscent of sparse coding [39], emerged without being explicitly enforced as in other approaches [3, 36, 39].

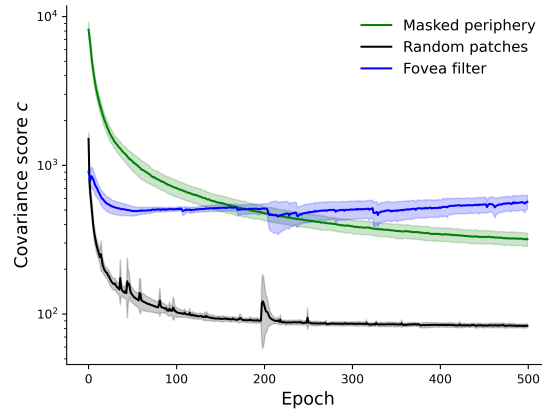


Fig. 5. Masked image modeling implicitly decorrelates latent space neurons. Shaded regions indicate the standard deviation across five randomly seeded runs.

4.3 Influence of Data Augmentation

Applying crop-and-resize augmentation during pretraining proved necessary for representation learning in the masked periphery condition. Without this augmentation technique, readout accuracy dropped from $67.9 \pm 0.4\%$ to $56.7 \pm 0.5\%$ (Fig. 4b). Biologically, this augmentation can be approximated through different viewing angles, especially since no assumption about temporal co-occurrence is made: differently augmented versions of an image are presented in different epochs. Interestingly, neither the foveal filter nor the random patches were affected by ablating the crop-and-resize transformation. Maintaining the position of the patch masks across epochs alone did not reduce readout accuracy ($70.3 \pm 0.9\%$), but in combination with ablation of the crop-and-resize augmentation, accuracy reduced to $62.5 \pm 0.8\%$. We conclude from this that the model requires exposure to a variety of prediction tasks from each object, whether through data augmentation or through changes in mask position.

4.4 Predicting Object vs. Background

Restricting the pretraining loss to the main object instead of the background, as described in section 3.5, did not affect linear probing accuracy negatively, suggesting that on-object predictions are sufficient for classification. While there was no substantial difference in readout accuracy when disregarding, as opposed to when using, loss signal from the background in the masked periphery condition (Fig. 6b), the network pretrained using random patch masks profited from disregarding the background, especially in early epochs (Fig. 6a).

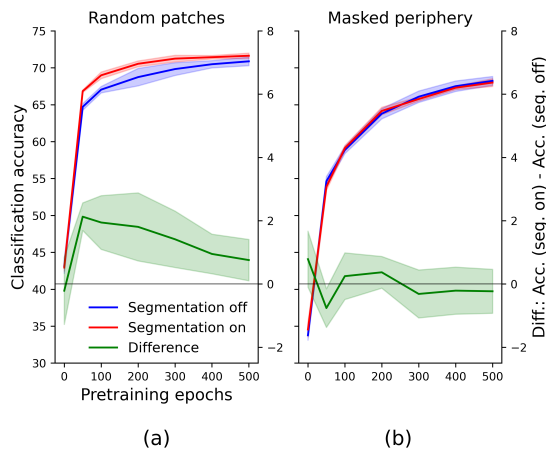


Fig. 6. Influence of presegmentation and masking strategy on training speed. (a) When using random patches, using presegmentation to weight the reconstruction loss accelerates training. (b) This is not the case when masking the periphery. Shaded regions indicate the standard deviation across five randomly seeded runs.

4.5 Reconstruction Quality

Beyond the network’s discriminative function, its generative capacity bears functional relevance, e.g., for counterfactual reasoning, predictions of occluded image content, and imagination [16]. An interesting effect from generative model learning can be observed in the networks pretrained with uniform (average colored) and blurry masks: These networks also reconstruct in locations in which no loss was calculated. While is to some degree expected when the masked area changes shape across image presentations (random patches), this is somewhat surprising in the masked periphery condition (Fig. 2, second column). Here, also the central region was reasonably reconstructed although the pretraining loss is indifferent to the network’s predictions. This holistic percept fits well with the proposed role of visual predictions in creating a stable visual representation [11, 16].

Across masking paradigms, reconstruction accuracy was uncorrelated with readout accuracy: while the foveal filter achieved the best reconstructions (Fig. 2), it performed poorly in linear probing (Fig. 4). Given a pretraining paradigm, however, longer training on the reconstruction task also improved readout (Fig. 6).

A third angle to analyze the generative capacity of the network stems from the fact that eye-movements are often preceded by covert attention shifts, which increase information sampling from these areas [40]. The sampled information can then be used to improve predictions about the expected image content. To test whether the model could exploit such a mechanism for improved reconstructions, we provided the model with a second circular input sampling area (covert attention) on top of the peripheral masking while constraining the error to the foreground (section 3.5). The additionally provided information indeed led to more truthful predictions (Fig. 7), i.e., reduced prediction errors (from $2.6\text{e-}2$ to $2.3\text{e-}2$), which ties the approach back to earlier theories of predictions as a stabilizing mechanism [11]. However, adding this sampling during pretraining, did not alter readout accuracy significantly, neither when setting the attention circle randomly nor when placing it on random positions of the main object.

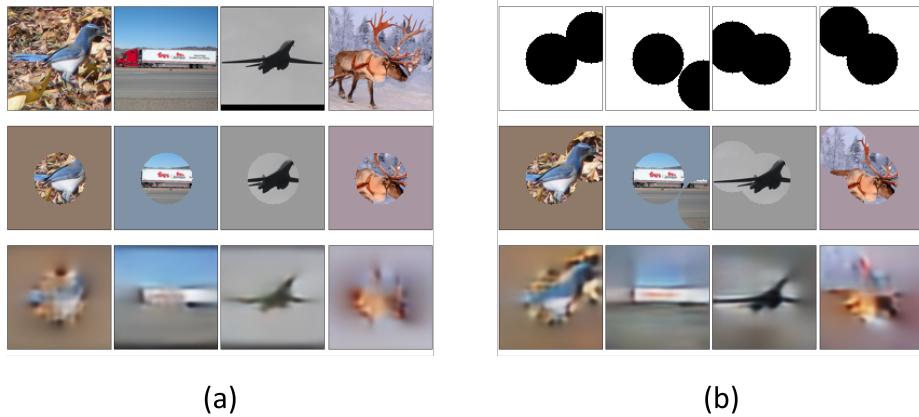


Fig. 7. Attention-guided predictions for stable perception. (a) Top row: ground truth. Middle row: input in the masked periphery condition with a masking ratio of 80%. Bottom row: reconstructions after pretraining. (b) Same as (a) with additionally provided information via a second, non-central input circle (covert attention). The top row depicts the input mask consisting of these two circular areas (fovea and attention). Adding covert attention improves reconstructions.

5 Conclusion

In this paper, we investigated key components of masked image modeling (MIM) through the lens of biological vision. As a similarly performant alternative to the random patch masks common in artificial representation learning [6, 21], we identified the more biologically plausible peripheral masking (Fig. 4a). Provided with differently augmented views of the input images (Fig. 4b), this approach does not pose restrictions on the temporal sequence in which inputs are encountered [8] or on knowledge about the spatial extent of an object to obtain negative samples [9]. An additional advantage of the employed approach in contrast to purely discriminative methods is learning of a generative model (Fig. 2, Fig. 7). A general requirement for high classification accuracy across all investigated masking strategies is strict intransparency of input masks (Fig. 4c), just as we sometimes do not perceive objects in our field of view while focusing on another point in space [10]. From a theoretical perspective, implicit decorrelation of latent space neurons (Fig. 5), together with previous observations of implicit invariance learning [41], connect the MIM framework to latent regularization SSL [3], where these objectives are explicitly enforced. This raises the question whether and how synergies could be efficiently exploited. We conclude that peripheral masking and prediction is a candidate mechanism for self-supervised learning in the brain, potentially in addition to previously proposed non-generative methods [8, 9]. These and other multi-view approaches [42, 43] have successfully conducted self-supervised learning with more local learning rules than backpropagation, raising the question whether the same can be done with MIM. Lastly, as primates employ eye-movements in a strategic and enactive way [27], an interesting extension would be to learn from multiple peripherally masked glimpses in a sequence through spatiotemporally masked videos [44].

Acknowledgements This project has received funding from the European Union’s Horizon 2020 Framework Programme for Research and Innovation under the Specific Grant Agreement No. 945539 (Human Brain Project SGA3 to C.P. and S.B.). We thank SURF (www.surf.nl) for the support in using the National Supercomputer Snellius and especially Thomas von Osch for the helpful discussions.

References

1. LeCun, Y.: A path towards autonomous machine intelligence version 0.9.2, 2022-06-27. Open Review 62(1) (2022)
2. Oord, A.v.d., Li, Y., Vinyals, O.: Representation learning with contrastive predictive coding. arXiv preprint arXiv:1807.03748 (2018)
3. Bardes, A., Ponce, J., LeCun, Y.: Vicreg: Variance-invariance-covariance regularization for self-supervised learning. arXiv preprint arXiv:2105.04906 (2021)

4. Grill, J.-B., Strub, F., Althé, F., Tallec, C., Richemond, P., Buchatskaya, E., Doersch, C., Avila Pires, B., Guo, Z., Gheshlaghi Azar, M.: Bootstrap your own latent—a new approach to self-supervised learning. *Advances in neural information processing systems* 33, 21271–21284 (2020)
5. Pathak, D., Krahenbuhl, P., Donahue, J., Darrell, T., Efros, A.A.: Context encoders: Feature learning by inpainting. In: *Proceedings of the IEEE conference on computer vision and pattern recognition*, pp. 2536–2544 (2016)
6. He, K., Chen, X., Xie, S., Li, Y., Dollár, P., Girshick, R.: Masked autoencoders are scalable vision learners. In: *Proceedings of the IEEE/CVF conference on computer vision and pattern recognition*, pp. 16000–16009 (2022)
7. Assran, M., Duval, Q., Misra, I., Bojanowski, P., Vincent, P., Rabbat, M., LeCun, Y., Ballas, N.: Self-supervised learning from images with a joint-embedding predictive architecture. In: *Proceedings of the IEEE/CVF Conference on Computer Vision and Pattern Recognition*, pp. 15619–15629 (2023)
8. Halvagal, M.S., Zenke, F.: The combination of Hebbian and predictive plasticity learns invariant object representations in deep sensory networks. *Nature Neuroscience* 26(11), 1906–1915 (2023)
9. Illing, B., Ventura, J., Bellec, G., Gerstner, W.: Local plasticity rules can learn deep representations using self-supervised contrastive predictions. *Advances in Neural Information Processing Systems* 34, 30365–30379 (2021)
10. Simons, D.J., Chabris, C.F.: Gorillas in our midst: Sustained inattentive blindness for dynamic events. *perception* 28(9), 1059–1074 (1999)
11. Crapse, T.B., Sommer, M.A.: The frontal eye field as a prediction map. *Progress in brain research* 171, 383–390 (2008)
12. Von Holst, E., Mittelstaedt, H.: Das Reafferenzprinzip: Wechselwirkungen zwischen Zentralnervensystem und Peripherie. *Naturwissenschaften* 37(20), 464–476 (1950)
13. Dayan, P., Hinton, G.E., Neal, R.M., Zemel, R.S.: The helmholtz machine. *Neural computation* 7(5), 889–904 (1995)
14. Rao, R.P., Ballard, D.H.: Predictive coding in the visual cortex: a functional interpretation of some extra-classical receptive-field effects. *Nature neuroscience* 2(1), 79–87 (1999)
15. Friston, K.: A theory of cortical responses. *Philosophical transactions of the Royal Society B: Biological sciences* 360(1456), 815–836 (2005)
16. Pennartz, C.M.: *The brain's representational power: on consciousness and the integration of modalities*. MIT Press (2015)
17. Kong, L., Ma, M.Q., Chen, G., Xing, E.P., Chi, Y., Morency, L.-P., Zhang, K.: Understanding Masked Autoencoders via Hierarchical Latent Variable Models. In: *Proceedings of the IEEE/CVF Conference on Computer Vision and Pattern Recognition*, pp. 7918–7928 (2023)
18. Tsao, T., Tsao, D.Y.: A topological solution to object segmentation and tracking. *Proceedings of the National Academy of Sciences* 119(41), e2204248119 (2022)
19. Brucklacher, M., Pezzulo, G., Mannella, F., Galati, G., Pennartz, C.M.: Learning to segment self-generated from externally caused optic flow through sensorimotor mismatch circuits. *bioRxiv preprint biorXiv:10.1101/2023.11.15.567170v2* (2023)
20. Hénaff, O.J., Koppula, S., Alayrac, J.-B., Van den Oord, A., Vinyals, O., Carreira, J.: Efficient visual pretraining with contrastive detection. In: *Proceedings of the IEEE/CVF International Conference on Computer Vision*, pp. 10086–10096 (2021)

21. Woo, S., Debnath, S., Hu, R., Chen, X., Liu, Z., Kweon, I.S., Xie, S.: Convnext v2: Co-designing and scaling convnets with masked autoencoders. In: Proceedings of the IEEE/CVF Conference on Computer Vision and Pattern Recognition, pp. 16133–16142 (2023)
22. Xie, Z., Zhang, Z., Cao, Y., Lin, Y., Bao, J., Yao, Z., Dai, Q., Hu, H.: Simmim: A simple framework for masked image modeling. In: Proceedings of the IEEE/CVF conference on computer vision and pattern recognition, pp. 9653–9663 (2022)
23. Lillicrap, T.P., Santoro, A., Marris, L., Akerman, C.J., Hinton, G.: Backpropagation and the brain. *Nature Reviews Neuroscience* 21(6), 335–346 (2020)
24. Whittington, J.C., Bogacz, R.: An approximation of the error backpropagation algorithm in a predictive coding network with local hebbian synaptic plasticity. *Neural computation* 29(5), 1229–1262 (2017)
25. Renninger, L., Coughlan, J., Verghese, P., Malik, J.: An information maximization model of eye movements. *Advances in neural information processing systems* 17 (2004)
26. Larochelle, H., Hinton, G.E.: Learning to combine foveal glimpses with a third-order Boltzmann machine. *Advances in neural information processing systems* 23 (2010)
27. Thompson, J.A., Sheahan, H., Summerfield, C.: Learning to count visual objects by combining” what” and” where” in recurrent memory. In: *NeuRIPS 2022 Workshop on Gaze Meets ML*, pp. 199–218 (2022)
28. Smith, A.T., Singh, K.D., Williams, A.L., Greenlee, M.W.: Estimating receptive field size from fMRI data in human striate and extrastriate visual cortex. *Cerebral cortex* 11(12), 1182–1190 (2001)
29. He, K., Zhang, X., Ren, S., Sun, J.: Deep residual learning for image recognition. In: *Proceedings of the IEEE conference on computer vision and pattern recognition*, pp. 770–778 (2016)
30. Coates, A., Ng, A., Lee, H.: An analysis of single-layer networks in unsupervised feature learning. In: *Proceedings of the fourteenth international conference on artificial intelligence and statistics*, pp. 215–223 (2011)
31. Purves, D., Augustine, G., Fitzpatrick, D., Hall, W., LaMantia, A., McNamara, J., White, L.: *Neuroscience, 3rd Edition*. Sinauer Associates (2004)
32. Perry, J.S., Geisler, W.S.: Gaze-contingent real-time simulation of arbitrary visual fields. In: *Human vision and electronic imaging VII*, pp. 57–69 (2002)
33. Jiang, M., Huang, S., Duan, J., Zhao, Q.: Salicon: Saliency in context. In: *Proceedings of the IEEE conference on computer vision and pattern recognition*, pp. 1072–1080 (2015)
34. Kingma, D.P., Ba, J.: Adam: A method for stochastic optimization. *arXiv preprint arXiv:1412.6980* (2014)
35. Barlow, H.B.: Possible principles underlying the transformation of sensory messages. *Sensory communication* 1(01), 217–233 (1961)
36. Zbontar, J., Jing, L., Misra, I., LeCun, Y., Deny, S.: Barlow twins: Self-supervised learning via redundancy reduction. In: *International conference on machine learning*, pp. 12310–12320 (2021)
37. Hayhoe, M., Ballard, D.: Eye movements in natural behavior. *Trends in cognitive sciences* 9(4), 188–194 (2005)
38. Yarbus, A.L.: *Eye movements and vision*. Plenum Press (1967)
39. Olshausen, B.A., Field, D.J.: Emergence of simple-cell receptive field properties by learning a sparse code for natural images. *Nature* 381(6583), 607–609 (1996)

- 40. Houtkamp, R., Spekreijse, H., Roelfsema, P.: A gradual spread of attention. *Perception & psychophysics* 65, 1136–1144 (2003)
- 41. Kong, X., Zhang, X.: Understanding masked image modeling via learning occlusion invariant feature. In: *Proceedings of the IEEE/CVF Conference on Computer Vision and Pattern Recognition*, pp. 6241–6251 (2023)
- 42. Löwe, S., O’Connor, P., Veeling, B.: Putting an end to end-to-end: Gradient-isolated learning of representations. *Advances in neural information processing systems* 32 (2019)
- 43. Siddiqui, S.A., Krueger, D., LeCun, Y., Deny, S.: Blockwise self-supervised learning at scale. *arXiv preprint arXiv:2302.01647* (2023)
- 44. Feichtenhofer, C., Li, Y., He, K.: Masked autoencoders as spatiotemporal learners. *Advances in neural information processing systems* 35, 35946–35958 (2022)